Environ Sci Pollut Res (2017) 24:26436–26443
DOI 10.1007/s11356-017-0249-y

RESEARCH ARTICLE

Hydrothermal synthesis of TiO_2 hollow spheres adorned with SnO_2 quantum dots and their efficiency in the production of methanol via photocatalysis

Sajan Ponnappa Chimmikuttanda[1] · **Amol Naik**[2] · **Maxwell Selase Akple**[3] · **Ravi Hethegowdanahally Rajegowda**[4]

Received: 4 May 2017 / Accepted: 19 September 2017 / Published online: 25 September 2017

Abstract TiO_2 hollow spheres and TiO_2 hollow spheres adorned with SnO_2 quantum dots were synthesized successfully under mild temperature and autogenous pressure using the hydrothermal route. X-ray diffraction, field emission scanning electron microscopy, scanning electron microscopy, transmission electron microscope, photoluminescence spectroscopy, and UV–vis spectroscopy were used to characterize the physical and chemical nature of the synthesized sample. The characterized samples were used in the photocatalytic applications to reduce the concentration of carbon dioxide in the presence of water under the influence of visible light. Our observation confirmed that with increasing SnO_2 content there is a tremendous change in the photocatalytic performance of the samples, due to free mobility of the electrons and holes and decline in charge recombination centers formed with the formation of nano-heterojunction between SnO_2 and TiO_2. The greater photocatalytic production of methanol was achieved using 2ST sample, i.e., 1.61 μmol/g/h which tends to decrease with an increase in SnO_2 content.

Responsible editor: Suresh Pillai

✉ Sajan Ponnappa Chimmikuttanda
sajan.saj@rediff.com

[1] Department of Studies in Environmental Science, University of Mysore, Manasagangothri, Mysore 570006, India

[2] Lead-Chemistry R and D VerdeEn Chemicals Pvt. Ltd., D-11, UPSIDC Industrial Area, Masoorie-Gulawati Road, Hapur District, Uttar Pradesh 201015, India

[3] Mechanical Engineering Department, Ho Technical University, P.O. Box HP 217, Ho, Ghana

[4] PG Department of Physics and Research Centre, Bharathi College, Bharathi Nagar, Mandya 571401, India

Keywords Photocatalytic · Hydrothermal · Hollow sphere · CO_2 reduction

The rapid growth in the industrialization has led to the overexploitation of fossil fuel, which serves as the source of energy, and has caused an increase in the concentration of carbon dioxide (CO_2) in the atmosphere. The increase in the concentration of CO_2 deteriorates the atmosphere, causing global warming. Immediate attention has to be paid to mitigate the risk associated with the atmosphere. Till date, environmental scientists have come out with many techniques to reduce the concentration of CO_2 such as bioenergy with carbon capture and storage (BECCS), electrochemical, photochemical, sequestration, etc., (Dowd et al. 2015; Hori, n.d.; Ogata et al. 1995; Stewart and Hessami 2005). However, these techniques have their drawback and limitations. In recent years, researchers have drawn their attention towards photocatalysis. Recently, the hot topic in the field of research is the CO_2 reduction via selective photocatalysts which takes place in the presence of H_2O to produce methane (CH_4), methanol (CH_3OH), formaldehyde (CH_2O), etc., (Cheung et al. 2016; Hong et al. 2013; Schmidt-Mende et al. 2013). So far materials such as Mn, Co, Fe, etc. have been effectively used as a photocatalyst in the CO_2 reduction (Cheung et al. 2016; Grodkowski and Neta 2002). Meanwhile, processing of semiconductor nanostructures has attracted the researchers as an important material for the photocatalytic application. Metal oxide and chalcogenide (sulfides) material such as TiO_2, ZnO, CeO_2, ZrO_2, SnO_2, CdS, ZnS, etc., has been used as catalytic material so far (Choi et al. 2010). Among these semiconducting materials, TiO_2 possess certain unique properties. Based on these properties such as maximum quantum yield, highest stability, low-cost, safe, enhanced photocatalytic ability compared with other semiconducting material, and can be

used effectively under weak solar irradiation, TiO_2 has been extensively used as a photocatalyst (Bavykin et al. 2006; Chen and Poon 2009; Fernandez et al. 1995; Fujishima et al. 2000; Hashimoto et al. 2005; Herrmann 2005). Tailoring of TiO_2 having special morphology such as 1D, 2D, and 3D materials of various size and their arrangement into different structures have proven to have an enhanced efficiency compared to other material (Choi et al. 2004; Lang et al. 2012; Meng et al. 2002; Passinger et al. 2007). Many articles related to TiO_2 structures having exposed (001) facet have reported having shown an enhanced photocatalytic activity (Ariga et al. 2009; Sajan et al. 2015). Improving the efficiency of the semiconductor photocatalytic material having special morphology through doping, deposition of foreign materials, composite materials etc., by employing suitable techniques such as sol-gel, radiofrequency sputtering (for thin film), chemical vapor deposition, hydrolysis, microwave hydrolysis, chemical precipitation, solid-state reaction, electrophoretic deposition, hydrothermal, solvothermal etc., (Lee et al. 2008; Li and Zhang 2012; Lyson-Sypien et al. 2017; Sangchay 2015; Yuan and Xu 2010) and their application in environmental remediation is a challenging field for the material scientists and environmentalists.

SnO_2 is an essential n-type semiconductor having wide bandgap. In recent years, TiO_2/SnO_2 composite have paid attention for its possible application in gas sensors, ceramic sensors, lithium storage, and photocatalytic application (Akurati et al. 2005; Chen et al. 2010; Chetri et al. 2014; Edelman et al. 2000; Kim et al. 2005; Lyson-Sypien et al. 2017; Sangchay 2016; Štengl et al. 2012). TiO_2/SnO_2 composites have proven themselves as one of the most important classes due to their various tunable physicochemical properties. Our present article focuses on the development of one such material employing the hydrothermal technique. Processing of TiO_2 hollow spheres adorned with SnO_2 quantum dots having nano-heterojunction and their application in the CO_2 reduction to CH_3OH in the presence of H_2O is the main focus of this article.

Materials and methods

Loba Chemicals Co. Ltd. and Qualignes Co. Ltd. were the suppliers of stannous oxide (SnO_2), titanium (IV) butoxide (TBT), isopropyl alcohol (C_3H_8O), and ammonium hydro-fluoride (NH_4HF_2). All the reagents were analytical grade (AR) and used without further purification. The post-treatment processes were performed using double-distilled water.

Hydrothermal synthesis of TiO_2 hollow spheres adorned with SnO_2 quantum dots

In the present work, commercial TBT acts as starting material. In a 100-ml Teflon liner, 3.4 ml of TBT followed by 25 ml of C_3H_8O was added and stirred using a magnetic stirrer for 2 h till the formation of a clear solution. Into this, 1.04 g of NH_4HF_2 was introduced and kept stirred for another 1 h. The Teflon liner was closed and kept in an autoclave and heated at 160 °C for 24 h. After the hydrothermal treatment, the autoclave was cooled suddenly using a compressed air jet to arrest the morphology of the crystal at the present set experimental condition. Opening the Teflon liner to this solution, SnO_2 was added of different weight ratios and kept stirred for another 1 h. The hydrothermal run was carried out at 160 °C for 2 h in the autoclave, with the liner closed and sealed within. After the hydrothermal run, the autoclave was removed out. Quenching of the autoclave before removing the liner was done to arrest the morphology of the crystals formed at the present set conditions. For comparison, the experiment was carried in the absence of SnO_2 separately. After removing the liner out, the solution was discarded to separate the powder sample. The powder was washed thoroughly using double-distilled water thrice to remove undesired compounds, and then ultrasonicated to avoid agglomeration. The powder sample was extracted by centrifuging and dried at a temperature of 35–40 °C in an oven. Based on the ratio of SnO_2:TiO_2, the samples named as 0ST, 0.5ST, 1ST, 2ST, 3WT, and 5ST where 0, 0.5, 1, 2, 3, and 5 represents the weight percentage of SnO_2 added.

Production of methanol via photocatalysis

The production of methanol via photocatalysis involves the generation of CO_2 in a closed self-made Pyrex container, followed by the reduction of CO_2 into energy products such as methane, methanol, formaldehyde, etc. In the present study, we have made use of a double-necked flask (Pyrex container) whose both ends are sealed with a silicone rubber plug, having a groove at one neck. In the production of methanol, 100 mg of the synthesized sample along with little-deionized water was taken and ultrasonicated thoroughly to disperse and avoid the agglomeration of the particles. The flask was kept in an oven, maintaining the temperature of 80 °C to form a thin film at the bottom. 120 mg of sodium bicarbonate then placed very next to the groove. The gaseous nitrogen was passed for 30 min to create an ambient condition inside the container, for 30 min. Later, both necks of the flask were sealed. 0.25 ml of 4 N HCl was carefully injected into the flask using the syringe in such a way that the HCl reacts only with the sodium bicarbonate placed before the groove producing CO_2 and H_2O. The flask was then exposed to UV light 350 W Xe arc lamp (using cut-off filter 380 nm), where the CO_2 present in the flask reduces and undergo a series of reaction to form energy products (Schmidt-Mende et al. 2013). 22 cms are the distance measured between the light source and the flask. After exposure to light for 1 h, from the container, 1 ml of evolved gas is extracted to perform the gas-phase recording. HP 5890 gas chromatography operational with flame

ionization detector was used to record the gaseous phase formed within the flask. In the present study, the major by-product obtained was methanol.

Instrumentation and characterization

The X-ray powder diffraction (XRD) pattern for the synthesized samples was recorded using Rigaku Miniflex X-ray diffractometer (Model IGC2, Rigaku Co. Ltd., Japan). The 2θ range was set between $10^{o}$and 80^{o}. The Fourier transform infrared spectrometry (FTIR) spectra of the synthesized samples were witness using JASCO-460 Plus, Japan. Comparison studies of the crystalline phase of the crystals along with JCPDS using PCPDF Win version revealed the crystallinity of the sample. High-resolution scanning electron microscope (SEM) TSL MSC-2200 was used to study the morphology of the samples. JEM-2100F electron microscope (JEOL, Japan) was used to conduct transmission electron microscopy (TEM) and high-resolution transmission electron microscopy (HRTEM) studies using a 200 kV accelerating voltage. UV-2550, Shimadzu, Japan (UV–visible spectrophotometer) was used to record the UV–visible absorbance spectra for the dry-pressed samples using $BaSO_4$ as a standard. F-7000, Hitachi, Japan, fluorescence spectrophotometer was used to measure the photoluminescence (PL) spectra of the samples at room temperature. HP 5890 gas chromatography equipped with flame ionization detector was used to record the conversion of CO_2 to CH_3OH formed during the photocatalysis.

Results and discussion

X-ray diffraction studies of TiO_2 hollow spheres and TiO_2 hollow spheres adorned with SnO_2 quantum dots

Figure 1 represents the powder XRD patterns of TiO_2 hollow spheres and TiO_2 hollow spheres adorned with SnO_2 quantum dots. Furthermore, for confirmation, we identified the crystalline phase of these samples and compared it with JCPDS file (PCPDFWIN-2.01). The XRD patterns for both TiO_2 hollow spheres and TiO_2 hollow spheres adorned with SnO_2 quantum dots match with PDF-21-1272 representing a tetragonal system, belonging to space group $I4_1/amd$. The XRD patterns reveal that all samples comprise of pure anatase phase. However, in TiO_2 hollow spheres adorned with SnO_2 quantum dots, there was no sign of new peaks corresponding to SnO_2 nor the shift in peak positions. This result suggests that the SnO_2 nanoparticles were probably attached to the surface of TiO_2 hollow spheres and had not incorporated into the lattice of TiO_2. Furthermore, based on the XRD studies, we noticed an increase in weight percentage of SnO_2; the intensity of (101) planes be likely to decrease, suggesting the deposition of SnO_2 on to (101) planes. The possible reason for this is the deposition of SnO_2 onto the surface of TiO_2 with weak crystallinity blocks the X-ray irradiation and coherent scattering. The percentage deposition of SnO_2 is comparatively less due to which there is no development of new peaks. However, the reduction in the peak intensity of (101) plane further confirms that the SnO_2 has been effective deposition onto the (101) plane of TiO_2 nanosheets present in the hollow spheres. It is noteworthy that the reduction occurs more on (101) facet of TiO_2 and hence has the affinity to gain more electrons than (001) facet (Xiong and Zhao 2012). However, compared to (101) facet, the (001) facet is more reactive towards reactant molecules for dissociative adsorption. The surface area of the (001) facet is comparatively high when compared to (101) facet probably due to which more number of the SnO_2 gets deposited onto the (101) plane. The deposition of SnO_2 onto the (101) plane leads to the formation of a heterojunction between SnO_2 and TiO_2 (001) facet, thereby separating the recombination of electron-hole pairs, which further enhances the photocatalytic activity.

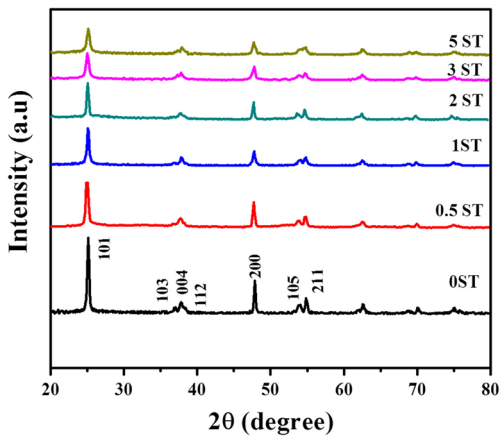

Fig. 1 XRD powder diffraction pattern of TiO_2 hollow spheres and TiO_2 hollow spheres adorned with SnO_2 quantum dots

FTIR studies of poly scale TiO_2 hollow spheres and TiO_2 hollow spheres adorned with SnO_2 quantum dots

The FTIR spectral studies for the synthesized samples were conducted to confirm the existence of SnO_2 in the samples. FTIR spectrum given in Fig. 2 represents the spectra of SnO_2, 0ST, 2ST, and 5ST samples. In the representative samples, the bands around the region 3400 cm^{-1} correspond to the O–H vibrating mode originated due to the absorption of water molecules which was added during the post-treatment process (Ramli et al. 2014). The band in the region 1600 and 2360 cm^{-1} represents the C–O stretching mode. The presence of C–O in the samples is due to absorption of atmospheric CO_2 (Liao et al. 2002). In all the samples, the region between 470 and 500 cm^{-1} are assigned to Ti–O stretch (Nolan et al. 2009). The formation of the new band at around 613 cm^{-1}in the IR spectra of the 2ST and 5ST samples signifies the O–Sn–

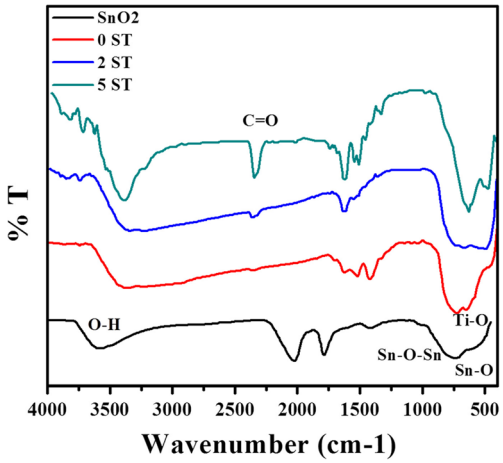

Fig. 2 FTIR studies of TiO_2 hollow spheres and SnO_2 quantum dots deposited TiO_2 hollow spheres

O vibration of SnO_2 (Yuan and Xu 2010). The peaks in the region 1335–1575 cm^{-1} possibly might correspond to residual isopropyl alcohol (Guo et al. 2007).

SEM and TEM studies of TiO_2 hollow spheres and TiO_2 hollow spheres adorned with SnO_2 quantum dots

The morphology and the structural features of the synthesized samples were analyzed through SEM and TEM micrographic studies (Fig. 3). The SEM images confirm that the arrangement of the TiO_2 crystals is spherical, ranging from 0.5–2 μm. A closer look at the SEM images illustrates that the present experimental condition is favorable to the formation of TiO_2 sheets of various sizes ranging from a few nanometers to micrometer, where the TiO_2 sheets are arranged one above the other forming spheres (Fig. 3b, c). It was noticed that these well-faceted nanocrystals have their unique growth habit where the flat, planar surface which is in a square shape is the {001} facets (Fig. 3d) and the edges/corners of the crystals having isosceles trapezoidal sidewall-like structure are the {101} surfaces (Fig. 3c). The HRTEM image (Fig. 3d) further reveals that the TiO_2 nanosheets (≃ 100 nm) are arranged to form a hollow cavity at the center of the sphere. During the hydrothermal run, the crystallites present in the middle region of the circular aggregates are smaller and less dense when compared to the crystallites present in the outer region. As a result, these crystallites dissolve and gets re-deposited onto the crystals present in the outer parts resulting in the formation of hollow spheres (Zeng 2007). On to the nanosheets, one can witness the deposition of tiny dots approximately in a range of 2–5 nm, which is nothing but the deposition of SnO_2 quantum dots (Fig. 3e). In Fig. 3f, the lattice spacing deliberated for the crystalline planes having 0.35 nm corresponds to (101) plane of TiO_2 nanosheet, which is in agreement with the XRD pattern where the (101) plane was prominent. The lattice spacing having 0.36 nm corresponds to (110) plane of SnO_2 measured from the crystalline plane. From Fig. 3f, one can witness the deposition of quantum dots of SnO_2 onto the (001) facet of the TiO_2 nanosheets. It should be noted that the (001) facets of anatase TiO_2 are believed to have a superior photocatalytic activity compared to other facets due to their increased surface energy and the 100% unsaturated Ti5c atoms (Yang et al. 2009; Yang et al. 2008). The deposition of SnO_2 onto (001) facet of TiO_2 nanosheets forms the heterogeneous junction between SnO_2 and TiO_2. It is understandable that the formation of a heterojunction between SnO_2 and TiO_2 due to the close contact between these two materials will make easy for the electron to transfer from TiO_2 crystals to SnO_2 particles when photo-excited. This phenomenon will lead to charge separation which is essential in enhancing the photocatalytic activity of the compound synthesized.

UV–vis diffuse reflectance spectra

The UV–vis absorption spectral studies on the synthesized samples were carried out (Fig. 4). According to our observation in the bare TiO_2 hollow spheres (0ST), the absorption edge lies at 380.3 nm which is in agreeing with the bandgap absorption of TiO_2 (3.26 eV). The addition of SnO_2 leads to the foremost increase in the absorption of the sample. However, with the change in SnO_2 concentration, there is an increase in the red-shift absorption of the samples up to 2%; beyond 2%, there is a decrease in the red-shift absorption. The possible reason for the red shift in the synthesized samples is the defects caused in TiO_2 crystals due to the addition of SnO_2, which causes lattice mismatch when deposited onto the TiO_2. Furthermore, to comprehend the role of SnO_2 in modifying the bandgap energy of TiO_2, the bandgap energy of the samples mentioned above were anticipated using Tauc plot and the extrapolation of the linear slope of photon energy. The change in the bandgap energy of the sample concerning the amount of SnO_2 added confirms the effective deposition of SnO_2 onto the TiO_2 hollow spheres. Notably, the bandgap energy of the samples decreases with increase in SnO_2 content. It is noteworthy that the bandgap energy for the representative samples is as follows, BG of 0ST > 1ST > 2ST < 5ST. Based on the bandgap studies, our work leads to a conclusion that the modification in the bandgap energy is probably as a result of the formation of new electron levels of Sn ions in the TiO_2 band structure which further confirms the effective deposition of SnO_2 onto TiO_2 hollow spheres. The deposition of SnO_2 on to the TiO_2 hollow spheres favors in free movement of electrons as well as it restrains the recombination of photogenerated electron and hole pairs.

PL spectral studies

It is well known that the PL emission results by the recombination of free carriers. PL is a nondestructive technique that can be used to measure the efficiency of charge carrier

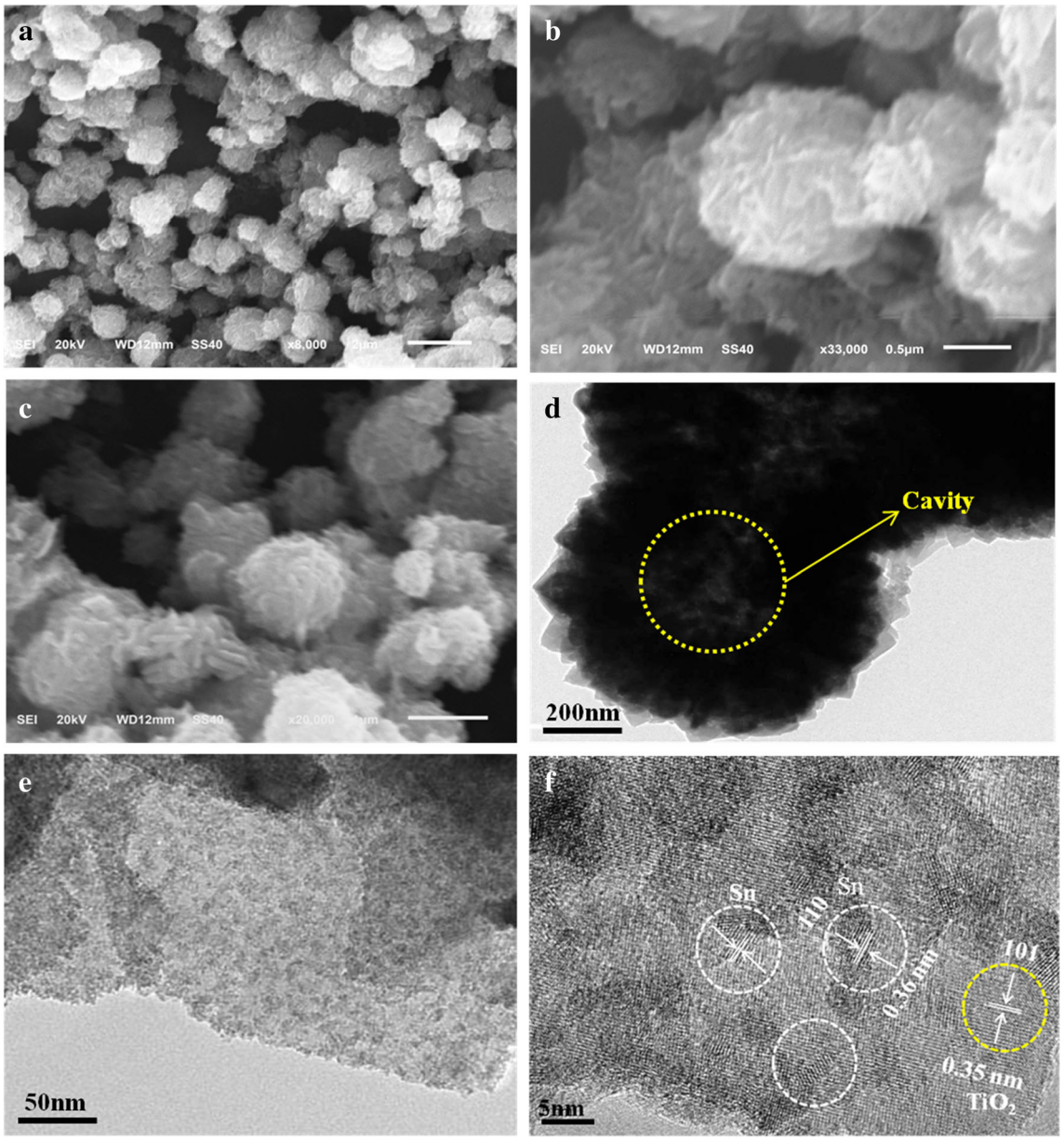

Fig. 3 SEM images of **a** TiO_2 hollow spheres, **b**, **c** high magnification SEM image of TiO_2 hollow spheres, **d** TEM images of TiO_2 hollow sphere showing cavity at the center, **e** HRTEM images showing the deposition of Sn quantum dots, and **f** HRTEM image showing lattice fringes 5ST sample

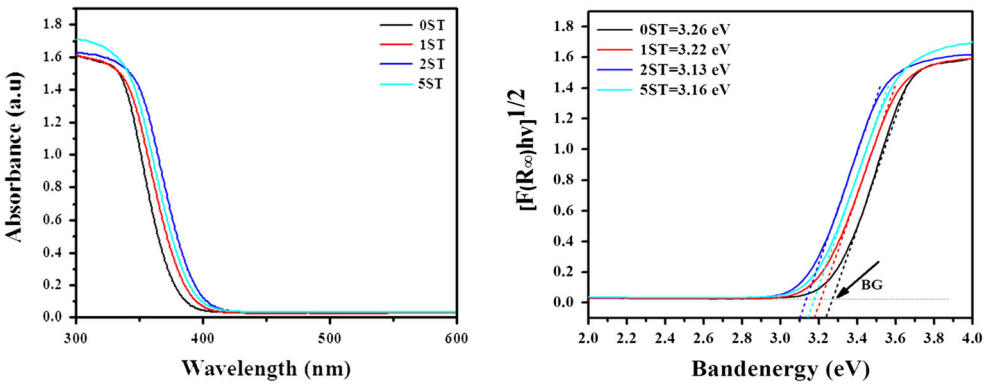

Fig. 4 UV–vis absorption spectra of TiO_2 hollow spheres and TiO_2 hollow spheres adorned with SnO_2 quantum dots

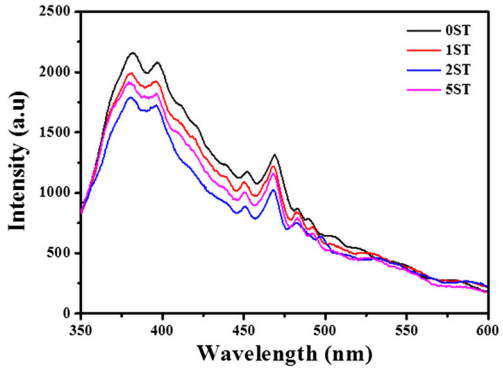

Fig. 5 PL spectra of TiO_2 hollow spheres and TiO_2 hollow spheres adorned with SnO_2 quantum dots

trapping, immigration, and transfer of electrons and also to know the possibilities of electron-hole pairs in the semiconductor particles. PL spectral studies for the TiO_2 hollow spheres and TiO_2 hollow spheres adorned with SnO_2 quantum dots were performed. Deposition of SnO_2 quantum dots onto TiO_2 hollow spheres has a significant effect on the PL intensity (Fig. 5). In our present study, we examined the PL emission spectra of 0ST, 1ST, 2ST, and 5ST in the range of 350–600 nm. The PL emission spectra of pure TiO_2 hollow sphere sample (Fig. 5) showed the existence of several peaks appearing at wavelength approximately 380, 395, 450, 468, 482, and 492 nm. The wavelengths of these peaks are equivalent to 3.26, 3.13, 2.75, 2.64, 2.57, and 2.52 eV. However, the PL emission spectra of TiO_2 hollow spheres and TiO_2 hollow spheres adorned with SnO_2 quantum dots samples showed almost the similar positions for most of the peaks, with the difference in PL intensities. The PL intensity decreases as the SnO_2 content increases and reaches the lower degree when SnO_2 content reached 2 wt%. On the other hand, when the concentration of SnO_2 content increased to 5 wt%, the intensity of PL begins to rise. The PL emission results from the recombination of excited electron and holes. As a result, a lower PL intensity indicates a lower recombination rate of electron/holes when exposed to light. In the present study, the 2ST sample shows lower intensity compared to the other samples, suggesting that the deposition of SnO_2 quantum dots onto TiO_2 hollow sphere has a major effect in reducing the recombination of electrons and holes and the possibility of showing high photocatalytic activity. The quick transfer of electrons between SnO_2 and TiO_2 results in improving the quantum efficiency by supplying more photogenerated electrons. When the concentration of SnO_2 deposition increases from 2 to 5%, the additional amount of SnO_2 quantum dots deposited onto TiO_2 behaves as charge recombination centers, increasing the intensity of the PL spectra having less photocatalytic efficiency.

The experimental results for the estimation of CO_2 reduction into CH_3OH via photocatalysis using the asprepared samples in the presence of water vapor under visible-light irradiation are as follows. The blank experiment conducted in the absence of light irradiation showed no significant reduction of CO_2 to CH_3OH. Figure 6 represents the comparison of CH_3OH evolution rates of all the samples under visible-light irradiation. We observed that the production of CH_3OH using 0ST sample was 1.14 μmol/g/h. On introducing SnO_2 in the sample, there was a change in the rate of CH_3OH production concerning the amount of SnO_2 added. The production of CH_3OH tends to increase up to a certain extent, and suddenly, there was a drastic decrease in the production of CH_3OH. The maximum production of CH_3OH was 1.61 μmol/g/h using the 2ST sample. As the SnO_2 content increases above 2 wt%, the production of CH_3OH tends to decrease. As the weight percent of SnO_2 increased to 5%, the production of methanol dropped to 0.31 μmol/g/h. The sudden decrease in photocatalytic activity of the samples with an increase in the SnO_2 content beyond 2% weight is due to the increase in charge recombination centers caused by the surplus addition of SnO_2. Therefore, a suitable content of SnO_2 is essential to optimize the photocatalytic activity of composites material; even the previous studies have proven this statement (Li and Li 2001).

The photocatalytic reduction of CO_2 to CH_3OH increases, as the SnO_2 content increases up to 2% weight. The increase in production of CH_3OH by 2ST sample illustrates the free

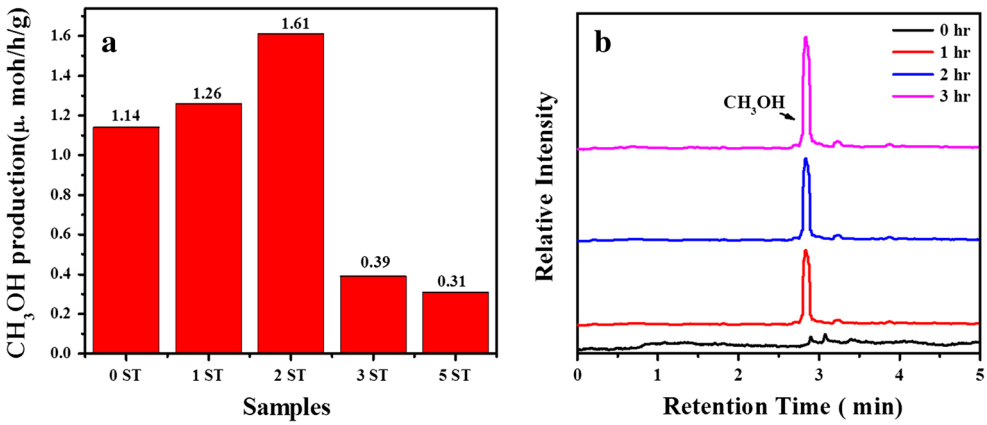

Fig. 6 **a** Photocatalytic reduction of CO_2 to methanol using TiO_2 hollow spheres and TiO_2 hollow spheres adorned with SnO_2 quantum dots. **b** GC spectra of reduction of CO_2 into CH_3OH using 2ST sample under different irradiation time

moment of electrons and holes onto the surface active sites during photocatalysis (Kudo and Miseki 2009). According to the basic principle of photocatalysis, when light falls on a photocatalyst like TiO_2, on excitation, the electrons move from valence band (VB) to conduction band (CB) leaving a hole in VB (Fujishima et al. 2000). Normally, these electrons and holes recombine quickly, resulting in a low photocatalytic activity. On introducing SnO_2 quantum dots, the formation of the heterojunction between the TiO_2 and SnO_2 reduces the recombination of an electron-hole pair in TiO_2. The free electrons generated in the TiO_2 tend to move from to the CB of SnO_2 since; the CB of TiO_2 is lower than the CB of SnO_2 (Fig. 7). This process leads to a formation of incomplete bonding on the TiO_2 side which in turn enhances the photocatalytic activity. Meanwhile, TiO_2 has the high electronic affinity when compared to the SnO_2. This property possessed by the TiO_2 favors in adsorption of more negative ions onto its surface during photocatalysis. The morphology of the synthesized sample also plays a major role in increasing the photocatalytic efficiency of the sample. The formation of nanosheets which arranged in the form of the hollow sphere is due to Ostwald ripening (Zeng 2007). These hollow spheres consist of a cavity within it, the cavity and the meso/macropores present in-between the nanosheets favors the light harvesting by allowing the light to pass through their pores, channels, and the hollow cavity which leads to the scattering of light. This process further increases the formation of electron and holes generated by exposure to light which further participates in photocatalysis (Yu and Zhang 2010).

To know the stability of the sample in the reduction of CO_2 to CH_3OH, the test for the production of CH_3OH carried for 3 cycles for 3 h. In the present study, methanol was the major by-product associated with a trace amount of formaldehyde and methane. Figure 6b gives the detail of the by-products formed during the reduction of CO_2 to CH_3OH using 2ST sample. At every 1-h interval, reading was taken. No detection of appreciable hydrocarbon compound found in the GC spectrum for the production of CH_3OH in the presence of photocatalyst and irradiation at 0 h. However, with an increase in the duration of exposure to light, there was an increase in the production of CH_3OH, suggesting that the CH_3OH so produced is via photocatalytic reactions on the photocatalyst.

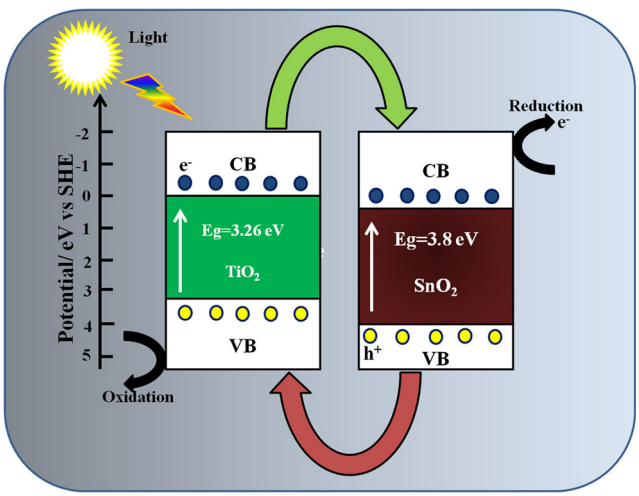

Fig. 7 Charge transfer between TiO_2 and SnO_2 heterojunction interface

Conclusion

Synthesis of TiO_2 hollow spheres and TiO_2 hollow spheres adorned with SnO_2 quantum dots was carried out under mild hydrothermal condition. The characterization studies demonstrated that the synthesized TiO_2 hollow spheres had been effectively adorned with SnO_2 quantum dots. The presence of SnO_2 has helped in tuning the bandgap as well as in the reduction of charge recombination. The photocatalytic reduction of CO_2 and converting them into energy product like CH_3OH proves the importance of the synthesized photocatalyst in environmental issues like global warming. Our study further confirmed that the efficiency in the production of CH_3OH depends on the added amount of SnO_2. The stability test revealed that the prepared catalyst could be reused for some cycles, which will reduce the cost of operation. It can be concluded that the use of TiO_2 hollow spheres adorned with SnO_2 quantum dots in the photocatalytic reduction of CO_2 or the production of CH_3OH of CO_2 will be a safe, economical, and environmentally benign technique to overcome the reduction of greenhouse gases which are the major culprits in causing the greenhouse effect and global warming.

Acknowledgments The authors wish to thank all who assisted in this work.

References

Akurati KK, Vital A, Hany R, Bommer B, Graule T, Winterer M (2005) One-step flame synthesis of SnO2/TiO2 composite nanoparticles for photocatalytic applications. Int J Photoenergy 7:153–161

Ariga H et al (2009) Surface-mediated visible-light photo-oxidation on pure TiO2(001). J Am Chem Soc 131:14670–14672

Bavykin DV, Friedrich JM, Walsh FC (2006) Protonated titanates and TiO2 nanostructured materials: synthesis properties, and applications. Advanced materials 18:2807–2824. https://doi.org/10.1002/adma.200502696

Chen J, Poon C-S (2009) Photocatalytic construction and building materials: from fundamentals to applications. Build Environ 44:1899–1906. https://doi.org/10.1016/j.buildenv.2009.01.002

Chen JS, Luan D, Li CM, Boey FYC, Lou XW (2010) TiO2 and SnO2@TiO2 hollow spheres assembled from anatase TiO2 nanosheets with enhanced lithium storage properties. Chem Commun 46:8252–8254

Chetri P, Basyach P, Choudhury A (2014) Structural, optical and photocatalytic properties of TiO2/SnO2 and SnO2/TiO2 core–shell nanocomposites: an experimental and DFT investigation. Chem Phys 434:1–10. https://doi.org/10.1016/j.chemphys.2014.02.007

Cheung PL, Machan CW, Malkhasian AYS, Agarwal J, Kubiak CP (2016) Photocatalytic Reduction of Carbon Dioxide to CO and HCO2H Using fac-Mn(CN)(bpy)(CO)3. Inorg Chem 55:3192–3198. https://doi.org/10.1021/acs.inorgchem.6b00379

Choi H, Al-Abed SR, Dionysiou DD, Stathatos E, Lianos P (2010) TiO2-based advanced oxidation nanotechnologies for water purification and reuse. Sustainability Science and Engineering, Vol 2. Elsevier B.V. https://doi.org/10.1016/S1871-2711(09)00208-6

Choi SY, Mamak M, Coombs N, Chopra N, Ozin GA (2004) Thermally stable two-dimensional hexagonal mesoporous nanocrystalline anatase, meso-nc-TiO2: bulk and crack-free thin film morphologies. Adv Funct Mater 14:335–344

Dowd A-M, Rodriguez M, Jeanneret T (2015) Social science insights for the BioCCS industry. Energies 8:4024–4042. https://doi.org/10.3390/en8054024

Edelman F et al (2000) Structural evolution of SnO2-TiO2 nanocrystalline films for gas sensors. Mater Sci Eng B 69–70:386–391

Fernandez A et al (1995) Preparation and characterization of Ti02 photocatalysts supported on various rigid supports (glass, quartz and stainless steel). Comparative studies of photocatalytic activity in water purification. Appl Catal B: Environ 7:49–63

Fujishima A, Rao TN, Tryk DA (2000) Titanium dioxide photocatalysis. J Photochem Photobiol C: Photochem Rev 1:1–21

Grodkowski J, Neta P (2002) Reduction of cobalt and iron corroles and catalyzed reduction of CO2. J Phys Chem A 106:4772–4778

Guo GS, He CN, Wang ZH, Gu FB, Han DM (2007) Synthesis of titania and titanate nanomaterials and their application in environmental analytical chemistry. Talanta 72:1687–1692. https://doi.org/10.1016/j.talanta.2007.03.039

Hashimoto K, Irie H, Fujishima A (2005) TiO2 photocatalysis: a historical overview and future prospects. Jpn J Appl Phys 44:8269–8285. https://doi.org/10.1143/jjap.44.8269

Herrmann JM (2005) Heterogeneous photocatalysis: state of the art and present applications In honor of Pr. R.L. Burwell Jr. (1912–2003), Former Head of Ipatieff Laboratories, Northwestern University, Evanston (Ill). Topics in catalysis 34:49–65. https://doi.org/10.1007/s11244-005-3788-2

Hong J, Zhang W, Ren J, Xu R (2013) Photocatalytic reduction of CO2: a brief review on product analysis and systematic methods. Anal Methods 5:1086. https://doi.org/10.1039/c2ay26270c

Hori Y (2008) Electrochemical CO2 reduction on metal electrodes. Vayenas C et al. (eds) modern aspects of electrochemistry. Springer, New York 42:89–189

Kim H-K et al (2005) Humidity sensing properties of nanoporous TiO2-SnO2 ceramic sensors. Bull Korean Chem Soc 26:1881–1884

Kudo A, Miseki Y (2009) Heterogeneous photocatalyst materials for water splitting. Chemical Society reviews 38:253–278. https://doi.org/10.1039/b800489g

Lang L, Wu D, Xu Z (2012) Controllable fabrication of TiO(2) 1D-nano/micro structures: solid, hollow, and tube-in-tube fibers by electrospinning and the photocatalytic performance. Chem 18:10661–10668. https://doi.org/10.1002/chem.201200378

Lee S-C, Yang Y-S, Chen H-L, Tsai C-C, Chuang C-S (2008) Properties of TiO2/SnO2 Co-deposited thin films deposited by radio frequency sputtering. The 4th international conference of Technological advances of thin film and surface coatings. Thin Films 1–9

Li J, Zhang L (2012) Synthesis of TiO2/SnO2 composite nanowire arrays via electrophoretic deposition method. Asian J Chem 24:4130–4132

Li XZ, Li FB (2001) Study of Au/Au3+-TiO2 photocatalysts toward visible photooxidation for water and wastewater Treatment. Environ Sci Technol 35:2381–2387

Liao LF, Lien CF, Shieh DL, Chen MT, Lin JL (2002) FTIR study of adsorption and photoassisted oxygen isotopic exchange of carbon monoxide, carbon dioxide, carbonate, and formate on TiO2. J Phys Chem B 106:11240–11245

Lyson-Sypien B et al (2017) Nanocrystalline TiO2/SnO2 heterostructures for gas sensing. Beilstein J Nanotechnol 8:108–122. https://doi.org/10.3762/bjnano.8.12

Meng Q-B, Fu C-H, Einaga Y, Gu Z-Z, Fujishima A, Sato O (2002) Assembly of highly ordered three-dimensional porous structure with nanocrystalline TiO2 semiconductors. Chem Mater 14:83–88

Nolan N, Pillai S, Seery M (2009) Spectroscopic investigation of the anatase-to-rutile transformation of sol−gel-synthesized TiO2 photocatalysts. J Phys Chem C 113:16151–16157. https://doi.org/10.1021/jp904358g

Ogata T, Yanagida S, Brunschwig BS, Fujita E (1995) Mechanistic and kinetic studies of cobalt macrocycles in a photochemical C02 reduction system: evidence of Co-C02 adducts as intermediates. J Am Chem Soc 117:6708–6716

Passinger S, Saifullah MSM, Reinhardt C, Subramanian KRV, Chichkov BN, Welland ME (2007) Direct 3D patterning of TiO2 using femtosecond laser pulses. Adv Mater 19:1218–1221. https://doi.org/10.1002/adma.200602264

Ramli ZAC, Asim N, Isahak WRW, Emdadi Z, Ahmad-Ludin N, Yarmo MA, Sopian K (2014) Photocatalytic degradation of methylene blue under UV light irradiation on prepared carbonaceous TiO2. Sci World J 2014:415136. https://doi.org/10.1155/2014/415136

Sajan CP, Wageh S, Al-Ghamdi AA, Yu J, Cao S (2015) TiO2 nanosheets with exposed {001} facets for photocatalytic applications. Nano Res 9:3–27. https://doi.org/10.1007/s12274-015-0919-3

Sangchay W (2015) Self-cleaning and antibacterial of E.coli properties of TiO2/SnO2 composites thin films. Eng J Chiang Mai Univ 22:31–37

Sangchay W (2016) The self-cleaning and photocatalytic properties of TiO2 doped with SnO2 thin films preparation by sol-gel method. Energy Procedia 89:170–176. https://doi.org/10.1016/j.egypro.2016.05.023

Schmidt-Mende L, Stolarczyk JK, Habisreutinger SN (2013) Photocatalytic reduction of CO2 on TiO2 and other semiconductors. Angewandte Chemie 52:7372–7408. https://doi.org/10.1002/anie.201207199

Štengl V, Grygar TM, Henych J, Kormunda M (2012) Hydrogen peroxide route to Sn-doped titania photocatalysts. Chem Cent J 6:2–18

Stewart C, Hessami M-A (2005) A study of methods of carbon dioxide capture and sequestration—the sustainability of a photosynthetic bioreactor approach. Energy Convers Manag 46:403–420. https://doi.org/10.1016/j.enconman.2004.03.009

Xiong Z, Zhao XS (2012) Nitrogen-doped titanate-anatase core-shell nanobelts with exposed {101} anatase facets and enhanced visible light photocatalytic activity. J Am Chem Soc 134:5754–5757. https://doi.org/10.1021/ja300730c

Yang HG et al (2009) Solvothermal synthesis and photoreactivity of anatase TiO2 nanosheets with dominant {001} facets. J Am Chem Soc 131:4078–4083

Yang HG et al (2008) Anatase TiO2 single crystals with a large percentage of reactive facets. Nature 453:638–641. https://doi.org/10.1038/nature06964

Yu J, Zhang J (2010) A simple template-free approach to TiO2 hollow spheres with enhanced photocatalytic activity. Dalton Trans 39:5860–5867. https://doi.org/10.1039/c0dt00053a

Yuan H, Xu J (2010) Preparation, characterization and photocatalytic activity of nanometer SnO2. Int J Chem Eng Appl 1:241–246

Zeng HC (2007) Ostwald ripening: a synthetic approach for hollow nanomaterials. Current Nanoscience 3:177–181